Channel State Reconstruction Using Multilevel Discrete Wavelet Transform for Improved Fingerprinting-Based Indoor Localization

Shih-Hau Fang, *Senior Member, IEEE*, Wei-Hsiang Chang, Yu Tsao, *Member, IEEE*, Huang-Chia Shih, *Member, IEEE*, and Chiapin Wang, *Senior Member, IEEE*

.

***Abstract*—Recently, channel state information (CSI) has been adopted as an enhanced wireless channel measurement instead of received signal strength (RSS) for indoor WiFi positioning systems. However, although CSI contains richer location information, a challenging problem is the severe dynamic range and fluctuation among the high-dimensional channels, which may degrade accuracy and cause overfitting problems. This paper proposes a novel algorithm for improved fingerprinting-based indoor localization. The proposed algorithm decomposes the CSI sequence using the multilevel discrete wavelet transform (MDWT) and normalizes the wavelet coefficients by employing histogram equalization. The robust features were then extracted by reconstructing CSI through the inverse MDWT of the normalized coefficients. We demonstrate the effectiveness of the proposed algorithm through experiments. The results show that the proposed algorithm outperforms traditional RSS, CSI, and two CSI-based algorithms, FIFS and MIMO.**

***Index Terms*—channel state, received signal strength, wavelet, mobile positioning, indoor fingerprinting.**

I. Introduction

Indoor localization has gained considerable attention over the last several years because position estimation is often required for various applications [1]–[6]. Because WiFi networks are widespread for Internet access, WiFi indoor localization has been a very active research problem [7]–[13]. Among the variety of positioning characteristics in WiFi networks, received signal strength (RSS) is commonly adopted because RSS characterizes the attenuation of radio signals during propagation, and reading RSS is compatible with existing WiFi-enabled devices [14]–[16]. However, accuracy and robustness are still fundamental problems in such Wi-Fi-RSS-based positioning systems [17]–[20].

In the 802.11a/g/n standard, WiFi networks used OFDM (orthogonal frequency division multiplexing) and MIMO (multiple input multiple output) techniques, where data are modulated on multiple channels in different frequencies and are transmitted simultaneously among multiple antenna pairs. The advantage of this technique is the significantly enhanced data throughput [21], [22]. In these systems, channel response can be extracted from the receivers in the format of channel state information (CSI), which reveals a set of channel measurements depicting the amplitudes and phases of every channel [23], [24]. There are various CSI-based applications recently. For examples, [25] tried to monitor breathing and heart rates while [26] attempted to detect fall in wireless networks. Unlike RSS, which provides an aggregated value for radio waves, CSI senses the channel responses, reporting amplitude and phase information of each channel for each antenna pair [27], [28]. This provides the opportunity to exploit the rich information in CSI to create higher-dimension location fingerprints.

Recently, CSI-based localization has attracted much research attention [27]–[32]. Some studies based on CSI have demonstrated an improved accuracy over RSS for indoor location estimation [33]–[38]. However, a challenging problem in CSI-based localization is the severe dynamic range and fluctuation among high-dimensional channels due to noise, multipath, and radio interference, even for stationary environments [24], [27], [28]. The studies in [34] proposed FIFS, which leverage both the frequency and spatial diversity and uses a correlation filter with the probability positioning algorithm. That is, FIFS represents the location by aggregating the power of all channels. However, the summation over all powers of CSI channels does not consider the variation within channels. A similar approach, namely, MIMO, was presented in [36], [37], in which the amplitude and phase value were subtracted for subsequent channels to generate the location fingerprint. Although this approach effectively extracts the relatively robust fingerprints owing to the subtraction process, the relative amplitude and phase may lose some location information. The works in [39] attempted to detect stationary and moving human by using a band-pass filter to catch the breathing patterns.

This paper proposes an enhanced CSI-based indoor positioning algorithm. The proposed algorithm include three steps: decomposition, normalization, and reconstruction. This study first applies the multilevel discrete wavelet transform (MDWT) [40]–[44] to decompose the full CSI sequence into

Shih-Hau Fang, Wei-Hsiang Chang, and Huang-Chia Shih are with the Department of Electrical Engineering, Yuan Ze University, Taiwan (Email: shfang@saturn.yzu.edu.tw, s994717@mail.yzu.edu.tw, and hcshih@saturn.yzu.edu.tw). Yu Tsao* is with the Research Center for Information Technology Innovation, Academia Sinica, Taiwan (yu.tsao@citi.sinica.edu.tw). Chiapin Wang is with the Department of Electrical Engineering, National Taiwan Normal University, Taiwan (chiapin@ntnu.edu.tw)

different parts. The wavelet coefficients are then normalized using histogram equalization (HEQ) [45], [46]. Afterward, we reconstruct CSI through the equalized coefficients with the inverse MDWT. Finally, the reconstructed features are adopted for fingerprinting-based positioning using a probabilistic approach. The proposed algorithm was applied in an indoor Wi-Fi environment, and real CSIs were measured for performance evaluation. By using the equalized CSIs, the proposed algorithm can achieve robust location estimation and avoid overfitting problems. Experimental results indicate that the proposed algorithm achieves notable improvements over RSS, CSI, MIMO, and FIFS in reducing the mean positioning error by 31.3%, 21.9%, 18.4%, and 20.8%, respectively.

II. Proposed Algorithm

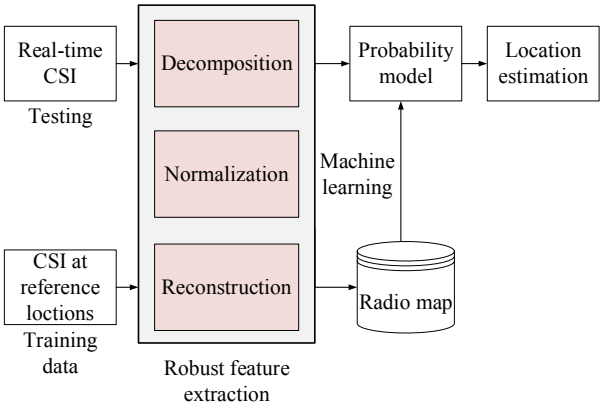

Fig. 1. Flowchart of proposed CSI-based indoor positioning system.

A. Problem Formulation

Because CSI reports the amplitude of each channel for each antenna pair, we assume that there are L directional links between each transmitter and receiver pair, and C channels are available for each link. A complete measured CSI signal in the MIMO wireless network is given as follows:

$$\mathbf{s} = [s_{11}, \ldots, s_{1C}, \ldots, s_{L1}, \ldots, s_{LC}]^{\mathrm{T}}. \quad (1)$$

To localize a user, a typical fingerprinting location algorithm estimates the likelihood of real-time CSI observations for all candidate locations and selects the one having maximum likelihood as the result [47]. Let $\Re$ be the entire set of reference locations; this CSI-fingerprinting localization problem can be formulated as

$$r^* = arg \max_{r \in \Re} P(\mathbf{s}|\Lambda_r), \quad (2)$$

where Λ_r is the probabilistic model of the r-th reference location, which can be obtained on the basis of the training data during the offline stage. A challenging problem in CSI-based localization is the severe dynamic range and fluctuation among high-dimensional CSI due to channel interference, noise, and multipath, even for stationary environments. To solve this problem, in this study a mechanism is designed to extract the robust positioning feature. Fig. 1 presents a flowchart of the proposed CSI-based indoor positioning system. The proposed algorithm, based on MDWT, includes three steps, decomposition, normalization, and reconstruction, as described in the following sessions.

B. Channel State Decomposition

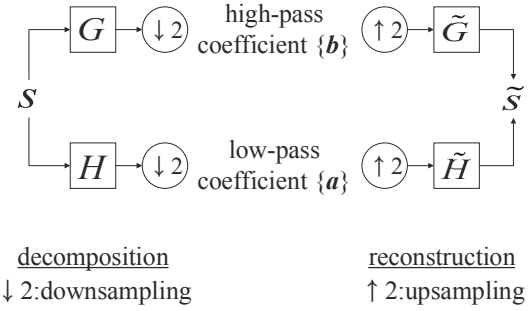

Fig. 2. Main idea of the DWMT procedure.

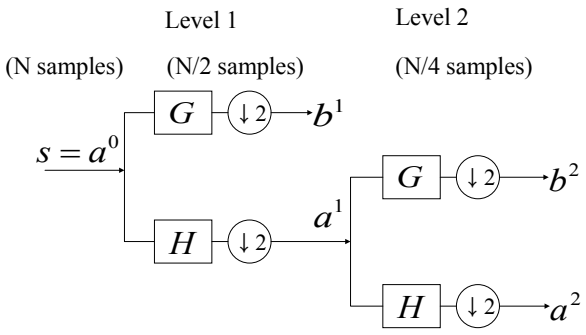

Fig. 3. Typical 2-level DWMT structure.

The proposed algorithm first applies MDWT to decompose the full CSI sequence. The measurements are represented by $\mathbf{s} = [s(1), \ldots, s(N)]^{\mathrm{T}}$ here for notation convenience, where $N = LC$. On the basis of MDWT, an input CSI sequence is decomposed into two sub delete space spaces, the low-pass and high-pass sequences, respectively, of the original data. The decomposition is implemented with two digital filters: high-pass filter G and low-pass filter H, which are derived from the scaling functions and the corresponding wavelets [44]. For example, if three-tap digital filters are considered, the transfer functions for the low-pass and high-pass components can be represented as $H(z) = h_0 + h_1 z^{-1} + h_2 z^{-2}$ and $G(z) = g_0 + g_1 z^{-1} + g_2 z^{-2}$, respectively, with the corresponding filter coefficients h_m and g_m. This can be represented as

$$s(n) = \sum_k a(k) h_k(n) + \sum_k b(k) g_k(n), \quad (3)$$

where $a(k)$ and $b(k)$ are the the low-pass and high-pass components of $s(n)$, respectively [40].

In the process of MDWT, a downsampling operation is used to decimate half of the filtered results. The reconstruction (synthesis) process is implemented with an upsampling operation and two different filters, $\tilde{G}$ and $\tilde{H}$. Exact recovery of the original data is possible if proper relationships hold among those filters [41], [42]. Figure 2 shows the classical implementation of decomposition and reconstruction for 1-level MDWT, where $\downarrow 2$ represents the down delete space sampling operation of factor 2, and $\uparrow 2$ represents the upsampling operation of factor 2 [43].

To achieve multi-level (multi-resolution) decomposition, MDWT can be implemented with the pyramid algorithm [44]. The decomposed coefficients at each resolution level are calculated as follows:

$$\begin{aligned} &\text{for (} j = 1 \text{ to } J) \\ &\text{for (} k = 0 \text{ to } N/2^j - 1) \\ &\left\{ \begin{array}{l} a^j(k) = \sum_{m=0}^{K-1} a^{j-1}(2k-m)h_m; \\ b^j(k) = \sum_{m=0}^{K-1} a^{j-1}(2k-m)g_m; \end{array} \right\} \end{aligned} \tag{4}$$

where j represents the current resolution level, K is the number of filter taps, $a^j(i)$ is the ith low-pass coefficient at the j-th level, $b^j(i)$ is the ith high-pass coefficient at the j-th level, and N is the length of the original input sequence a^0. Figure 3 shows a two-level MDWT implementation structure based on the pyramid algorithm. The output coefficients at each resolution level are calculated by using the low-pass coefficients of the previous level and are decimated by two. The detailed designs of filters G, H, $\tilde{G}$, and $\tilde{H}$ can be found in the literature [42], [48]–[50].

C. Wavelet Coefficient Normalization

After decomposing CSI into multi-resolution components, this study applies the HEQ technique to normalize the derived wavelet coefficients (i.e., converting the coefficients into a reference). The purpose of HEQ is to provide a transformation that converts the probability density function of an original variable into a reference probability density function [46], [51]. Let w_0 and w_1 be the original and reference variables, respectively, with distributions $p_0(w_0)$ and $p_1(w_1)$. A transformation, $w_1 = F(w_0)$, equalizes the probability distribution according to the following expression:

$$p_1(w_1) = p_0\left(G\left(w_1\right)\right) \frac{\partial G\left(w_1\right)}{\partial w_1}, \tag{5}$$

where $G\left(w_1\right)$ is the inverse function of $F\left(w_0\right)$. The relationship between the cumulative probability density functions (CDFs) associated with these probability distributions is given by

$$C_0(w_0) = C_1(F(w_0)), \tag{6}$$

where $C_1(F(w_0))$ and $C_0\left(w_0\right)$ are the CDFs of the reference and original distributions, respectively. The transformation $w_1 = F(w_0)$, which converts the distribution $p_0(w_0)$ into the reference distribution $p_1(w_1)$, also converts the cumulative probability $C_0\left(w_0\right)$ into $C_1\left(w_1\right)$. Hence, the transformation function $F\left(w_0\right)$ converting $p_0(w_0)$ into $p_1(w_1)$ is expressed as

$$w_1 = F\left(w_0\right) = C_1^{-1}\left[C_0\left(w_0\right)\right], \tag{7}$$

where C_1^{-1} denotes the inverse function of the CDF $C_1\left(w_1\right)$, specifying the value w_1 that corresponds to a certain cumulative probability.

Now, assume that the derived wavelet coefficients $\mathbf{w}$ (original variables) are represented by

$$\mathbf{w} = \{\mathbf{a}^J, \alpha^J\mathbf{b}^J, \alpha^{J-1}\mathbf{b}^{J-1}, \ldots, \alpha^1\mathbf{b}^1\}, \tag{8}$$

where $\mathbf{a}^j$ and $\mathbf{b}^j$ represent the j-th level low-pass and high-pass coefficients, and α^j is a scalar that takes values of either one or zero, indicating whether or not the j-th high-pass coefficients are preserved. The indicator of $\mathbf{a}^J$ is one because the last low-pass coefficients are always preserved according to MDWT theory. For example, $\alpha^1 = 0$ means that $\mathbf{b}^1$ is a zero vector ($\mathbf{b}^1$=$\mathbf{0}$). If J=2 and $\alpha^1 = 0$, the preserved coefficients reduce to $\{\mathbf{a}^2, \mathbf{b}^2, \mathbf{0}\}$. For simplification, a reorganized vector $\mathbf{w}$ consisting of all Q coefficients is then defined as $\mathbf{w} = [w_1, w_2, \ldots, w_Q]$. Given $\mathbf{w}$, normalized wavelet coefficients based on Eq. (7) are obtained using

$$\tilde{w}_i = F\left(w_i\right) = C_{ref}^{-1}\left[C_{\mathbf{w}}\left(w_i\right)\right], \tag{9}$$

where C_{ref}^{-1} is the inverse of the reference CDF, $C_{\mathbf{w}}$ represents the CDF of the sequence $\mathbf{w}$, F is the equalized transformation, and $\tilde{w}_i$ is the i-th normalized coefficient. One can compute $C_{\mathbf{w}}(w_i)$ with the empirical distribution function, which is the number of observations less than or equal to w_i divided by the total numbers. Finally, we may obtain the normalized coefficients as $\tilde{\mathbf{w}} = \{\tilde{\mathbf{a}}^J, \tilde{\mathbf{b}}^J, \tilde{\mathbf{b}}^{J-1}, \ldots, \tilde{\mathbf{b}}^1\}$.

This study uses a typical Gaussian distribution as the reference C_{ref} for normalization. In this case, the inverse CDF can be expressed as

$$C_{ref}^{-1}(z) = \left[\Phi\left(\frac{z-\mu}{\sigma}\right)\right]^{-1} = \left[\Phi\left(z'\right)\right]^{-1}, \tag{10}$$

where z is a reference Gaussian variable with mean μ and standard deviation σ. The variable z' is the normalized Gaussian variable and Φ is an error function expressed as

$$\Phi\left(z'\right) = \frac{1}{\sqrt{2\pi}} \int_{-\infty}^{z'} e^{-u^2/2} du \tag{11}$$

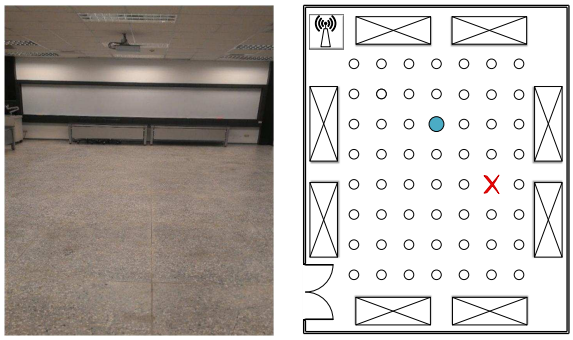

(a) Photo of test-bed. (b) layout of test-bed.

Fig. 4. Experimental setup.

D. Channel State Reconstruction

After obtaining the normalized multi-resolution wavelet coefficients, we attempt to reconstruct the CSI sequence as

$$\tilde{s}(n) = \sum_{k} \tilde{a}(k)\tilde{h}_k(n) + \sum_{k} \tilde{b}(k)\tilde{g}_k(n) \tag{12}$$

As with decomposition, the reconstructed MDWT coefficients at each resolution level can be represented as follows [44]:

$$\begin{aligned} &\text{for } (\ j = J \text{ to } 1) \\ &\text{for } (\ k = 0 \text{ to } N/2^j - 1) \\ &\left\{ \tilde{a}^{j-1}(2k-1) = \sum_{m=0}^{K/2-1} \tilde{a}^j(k-m)\tilde{h}_{2m+1} + \right. \\ &\sum_{m=0}^{K/2-1} \tilde{b}^j(k-m)\tilde{g}_{2m+1}; \\ &\tilde{a}^{j-1}(2k) = \sum_{m=0}^{K/2-1} \tilde{a}^j(k-m)\tilde{h}_{2m} + \\ &\left. \sum_{m=0}^{K/2-1} \tilde{b}^j(k-m)\tilde{g}_{2m}; \right\} \end{aligned} \tag{13}$$

Finally, after reconstructing coefficients to the first resolution level ($\tilde{s} = \tilde{a}^0$), the reconstructed CSIs are adopted for positioning using a probabilistic approach follows:

$$r^* = arg \max_{r \in \Re} P(\tilde{\mathbf{s}}|\Lambda_r) \tag{14}$$

Note that the proposed algorithm was applied for both online measurements and offline training CSIs. This procedure is required for the consistence of likelihood computation, as indicated in Fig. 1.

III. Experimental Results and Analysis

A. Experimental Setup

This study conducted experiments in a classroom of the telecommunications building at Yuan-Ze University. Figure 4(a) shows the photo of the location where the experiments were performed, while the circles in Fig. 4(b) indicate the 56 training locations. One AP with two transmitted antennae was deployed at the corner and the size of the test-bed was 140 m^2. After installing the Linux 802.11n driver, which is built on the Intel Wi-Fi Wireless Link 5300 MIMO radios [23], [27], the gain and phase of the signal path between a single transmit−receive antenna pair is available in the measured device. In the experiments, the laptop measured CSIs using three receiver antenna, and thus there were 6 links available as positioning features ($L = 6$). Each reported channel state contains 30 subcarrier channel groups ($C = 30$). Each channel state matrix entry is a complex number and only the magnitudes were used in this study. We select the biorthogonal wavelet (bior 2.2) [42], [49], [50] with a two-layer structure (J=2) to perform MDWT.

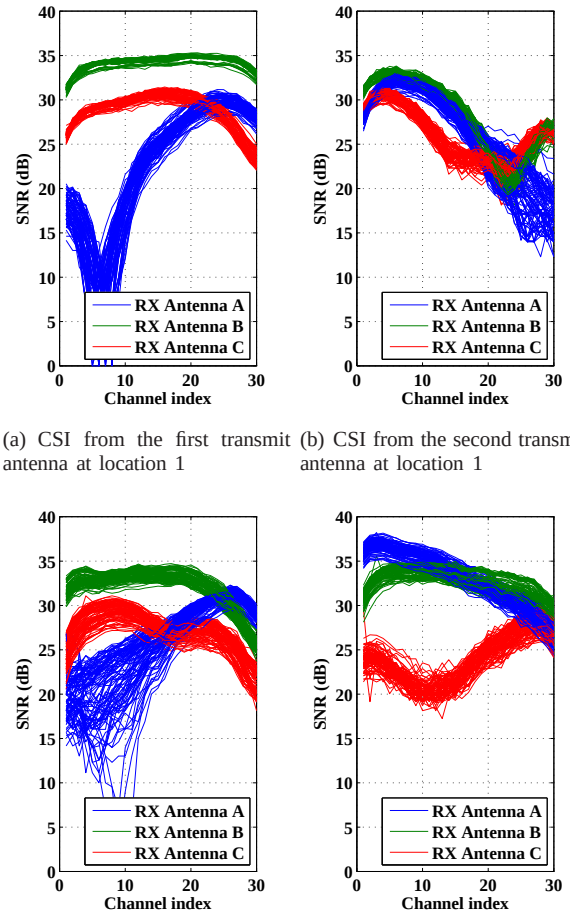

(a) CSI from the first transmit antenna at location 1 (b) CSI from the second transmit antenna at location 1

(c) CSI from the first transmit antenna at location 2 (d) CSI from the second transmit antenna at location 2

Fig. 5. The measured six-link CSI signals over 100s at two different locations.

Figure 5(a) shows the realistic CSI measurements from one transmit antenna, while Fig. 5(b) shows them from an alternative transmit antenna. In both figures, CSIs are measured over 100s at a fixed location, indicated by a blue

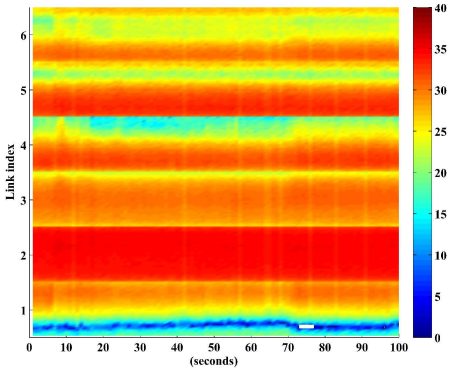

(a) Spectrogram of CSIs at location 1

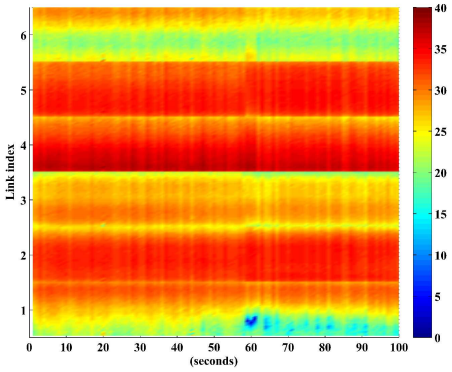

(b) Spectrogram of CSIs at location 2

Fig. 6. The spectrogram of CSIs at two different locations.

circle in Fig. 4(b). The wider curve represents the higher time variation of an antenna pair. Similarly, Figures 5(c) and 5(d) show the measured CSI at a distinct location. Figure 5 clearly reveals the changing CSI patterns measured from two different locations. It indicates the possibility of determining the location on the basis of CSI. However, CSI patterns contains uncertainty, especially when dramatic variation appears in some channels, as shown in Fig. 5(b) (channels 25−50) and Fig. 5(c) (channels 6−11). In this study, we use a 2-s sliding window performing a time average to smooth the CSI values. Figure 6 shows the spectrogram of CSIs at two different locations, showing that a mechanism to compensate for the high dynamic range across the entire channels is necessary.

B. Performance Evaluation

Figure 7 displays the mean positioning error of six different algorithms, including RSSI, CSI, HEQ, MIMO, FIFS, and the proposed algorithm versus number of channels. Note that the RSSI and FIFS methods are constant because the dimensions are fixed, and the HEQ approach indicates the direct normalization of CSI. This figure first shows that the mean positioning error generally decreases as the number

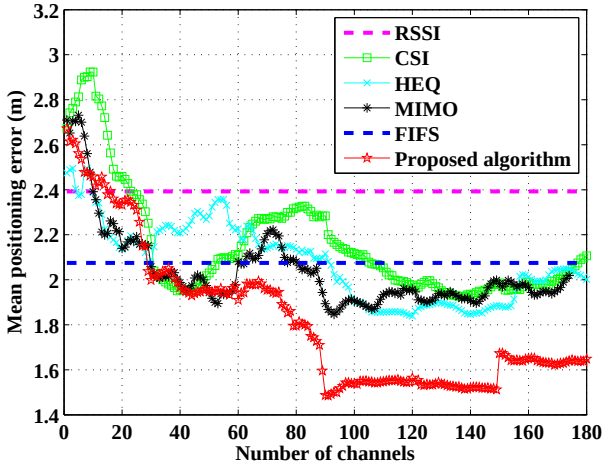

Fig. 7. Performance comparison between different positioning algorithms.

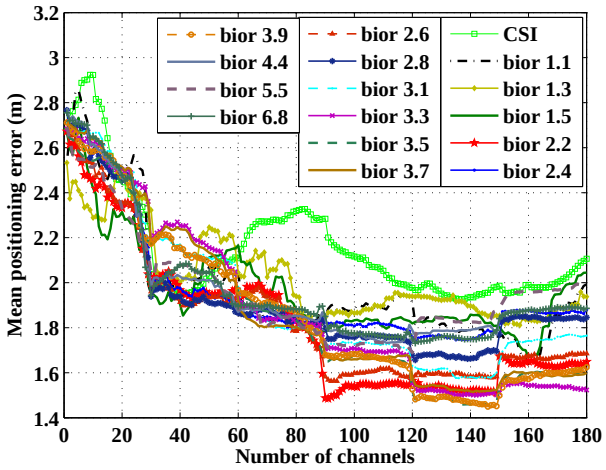

Fig. 8. Impact of different coefficients of the biorthogonal wavelets.

of channels increases. Second, this figure indicates the effectiveness of the CSI-based approaches, which considerably reduce the error compared with RSS as long as more than 20 channels are used.

More importantly, Fig. 7 shows that the proposed algorithm outperforms traditional methods, reducing the mean localization error by 31.3%, 21.9%, 18%, 18.4% and 20.8%, compared to RSSI, CSI, HEQ, MIMO, and FIFS, respectively, using full channels. The best performance occurred while using three links (1.48 m), with relative error reduction rates of 38% and 22% as compared to RSSI (2.39 m) and MIMO (1.89 m), respectively. The results indicate that the proposed algorithm is capable of achieving robust location estimation, by reconstructing the CSI sequence on the basis of the discrete wavelet transform with histogram normalized coefficients.

Table I reports five numerical error measures including the average, 50%, 67%, 90% percentile errors, and STD (standard

TABLE I
PERFORMANCE COMPARISON BETWEEN DIFFERENT ALGORITHMS.

3 links (90 channels)					
Methods\Performance	Average	50^{th}	67^{th}	90^{th}	STD
RSS	2.39	2.22	2.79	4.42	1.36
CSI	2.28	2.00	3.60	5.82	2.25
HEQ	2.11	2.00	3.00	5.00	2.05
MIMO	1.89	1.41	2.36	4.99	1.86
FIFS	2.07	1.88	2.43	4.47	2.05
Proposed algorithm	1.48	1.40	2.00	3.16	1.48
4 links (120 channels)					
Methods\Performance	Average	50^{th}	67^{th}	90^{th}	STD
RSS	2.39	2.22	2.79	4.42	1.36
CSI	1.97	1.41	2.23	5.09	2.08
HEQ	1.83	1.41	2.23	4.47	1.90
MIMO	1.95	1.41	3.03	4.99	1.92
FIFS	2.07	1.88	2.43	4.47	2.05
Proposed algorithm	1.56	1.41	2.03	3.46	1.58
5 links (150 channels)					
Methods\Performance	Average	50^{th}	67^{th}	90^{th}	STD
RSS	2.39	2.22	2.79	4.42	1.36
CSI	1.98	1.41	2.23	5.09	2.10
HEQ	1.88	1.41	2.23	4.47	1.92
MIMO	1.98	1.41	2.83	4.98	1.93
FIFS	2.07	1.88	2.43	4.47	2.05
Proposed algorithm	1.67	1.39	2.23	4.47	1.71
6 links (180 channels)					
Methods\Performance	Average	50^{th}	67^{th}	90^{th}	STD
RSS	2.39	2.22	2.79	4.42	1.36
CSI	2.10	1.41	2.82	5.09	2.16
HEQ	2.00	1.41	2.95	5.09	2.02
MIMO	2.01	1.41	3.16	4.99	1.96
FIFS	2.07	1.88	2.43	4.47	2.05
Proposed algorithm	1.64	1.23	2.16	4.47	1.70

deviation) for six algorithms with four different number of links. This table shows that, no matter how many links the proposed algorithm uses, its robustness is superior to that of other methods. This again demonstrates the effectiveness of the proposed mechanism.

Figure 8 shows the impact of different coefficients of the biorthogonal wavelets on positioning errors. The results show that the errors are almost always reduced in these wavelet-coefficient setups. In Fig. 8, bior 3.3 performs the best using full 180 channels, whereas bior 2.2 achieves the lowest positioning error with 90 channels. This confirms that the proposed algorithm with the biorthogonal wavelets can properly reconstruct the CSI patterns, which is a robust feature in location systems.

Next, Fig. 9 shows a box plot of the statistical positioning errors with three different wavelets, biorthogonal, Daubechies, and symlets under 10 coefficients in the proposed positioning system. Each red line represents the median, the blue boxes represent the 25th and 75th percentile values, and the dashed lines represent the maximum and minimum values. This figure shows that the biorthogonal

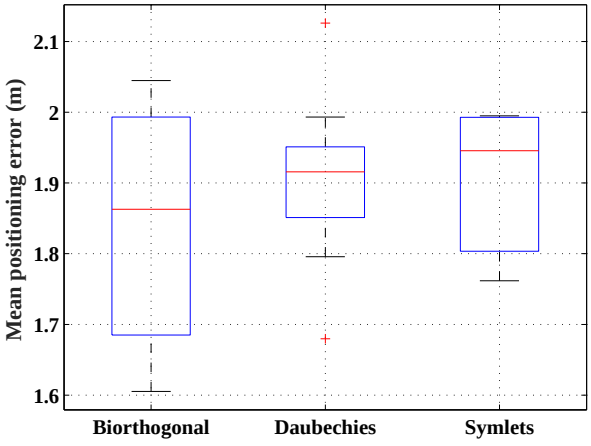

Fig. 9. Impact of selection of different wavelets.

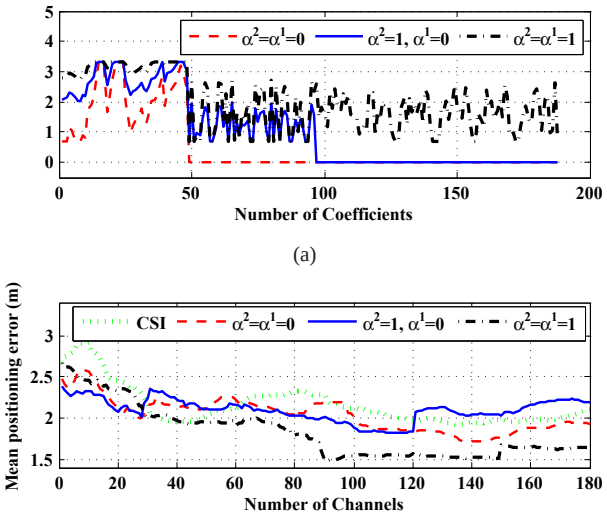

Fig. 10. The impact of different preserved configurations on (a)normalized wavelet coefficients and (b)mean positioning errors.

wavelet presents the minimum median error, whereas the Daubechies and symlets wavelets exhibits the lower dynamic range. That explains why we select biorthogonal wavelets to reconstruct CSI vectors in this study. Finally, Fig. 10 shows the impact of parameters α^j on coefficient normalization and mean positioning errors. Fig. 10(a) shows the normalized wavelet coefficients based on three parameter configurations $(\alpha^1 = \alpha^2 = 0)$, $(\alpha^1 = \alpha^2 = 1)$, and $(\alpha^1 = 1, \alpha^2 = 0)$. Fig. 10(b) shows the mean positioning over 180 channels, where the performance of CSI is also reported as a benchmark. The results show that the configuration $(\alpha^1 = \alpha^2 = 1)$ achieves the best performance. That means that the high-pass coefficients still contribute to the positioning system even in the presence of a highly dynamic range. After the normalization, the channel variation was significantly

alleviated, making the reconstruction CSI a robust positioning feature. Note that the lengths of the one-level wavelet are half of the original coefficients because the down-sampling process is conducted in the MDWT procedure. That is, the advantage of the other configurations is that the amount of data transmission can be reduced. For example, for the configuration ($\alpha^1 = \alpha^2 = 0$), only one-fourth of the coefficients are preserved to reconstruct CSI. The experiments and analysis reveal the effectiveness of the proposed algorithm in providing robust indoor localization.

Fig. 11 shows the impact of different layer numbers of MDWT on positioning errors. Results show that level 2 performs the best using between 120 and full 180 channels, while levels 4-7 provide comparable performance with level 2 between 90 and 120 channels. That explains why we select level 2 to perform MDWT and reconstruct CSI in the experiments. Finally, Fig. 12 compares different parameter normalization methods with HEQ, including two typical mean normalization (MN) and mean and variance normalization (MVN) methods. Figures 12(a) and 12(b) show the positioning errors based on three normalization methods under (α^2=α^1=1) and (α^2=1, α^1=0) parameter setups, respectively. These figures show that HEQ generally achieves the best performance because it normalizes higher order statistics, as compared to MN and MVN. The results again demonstrate the ability of HEQ to make the reconstructed CSI a robust positioning feature.

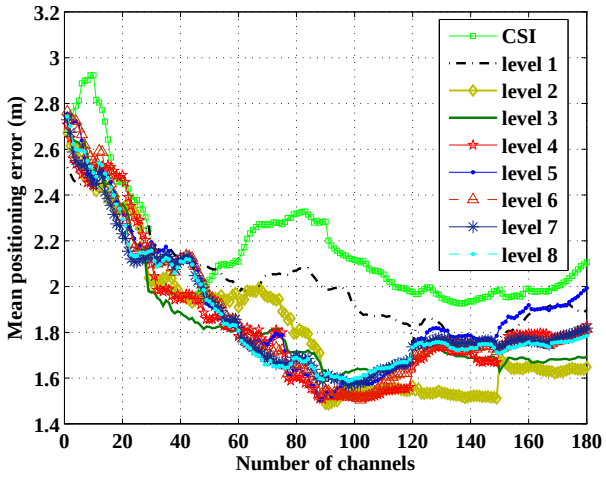

Fig. 11. Impact of selection of different layer numbers of MDWT on positioning errors.

IV. Conclusion

Because of the rich information in the physical layer of WiFi networks, CSI-based localization has attracted much attention. This study proposes an improved CSI-based indoor localization algorithm. By reconstructing CSI through inverse MDWT with HEQ-normalized wavelet coefficients, the proposed algorithm extracts the robust positioning features from CSI and achieves enhanced location estimation accuracy. Experimental results indicate that the proposed algorithm achieves notable improvements over RSSI, CSI, MIMO, and FIFS in reducing the mean positioning error by 31.3%, 21.9%, 18.4%, and 20.8%, respectively.

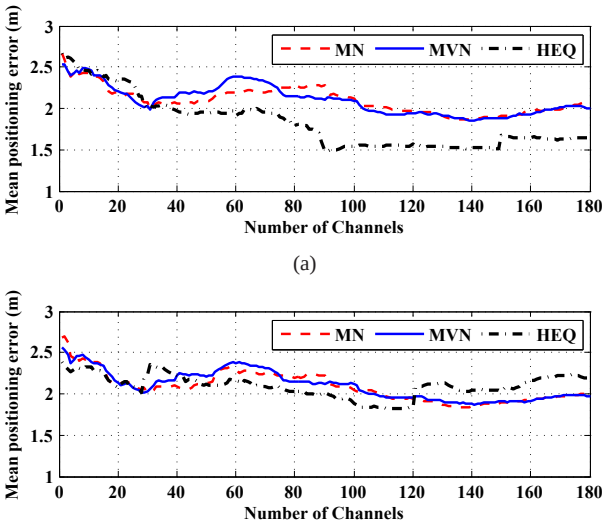

Fig. 12. The impact of different normalization methods on wavelet coefficients under (a)(α^2=α^1=1) and (b)(α^2=1α^1=0) parameters setups.

Acknowledgment

The authors would like to thank the financial support provided by Ministry of Science and Technology (102-2221-E-155-006-MY3 and 105-2221-E-155-013-MY3).

References

[1] Y. Gu, A. Lo, and I. Niemegeers, "A Survey of Indoor Positioning Systems for Wireless Personal Networks," *IEEE Communications Surveys & Tutorials*, vol. 11, no. 1, pp. 13–32, 2009.

[2] Q. Jiang, Y. Ma, K. Liu, and Z. Dou, "A Probabilistic Radio Map Construction Scheme for Crowdsourcing-Based Fingerprinting Localization," *IEEE Sens. J.*, vol. 16, pp. 3764–3774, May 2016.

[3] G. Deak, K. Curran, and J. Condell, "A Survey of Active and Passive Indoor Localisation Systems," *Computer Communications*, vol. 35, no. 16, pp. 1939–1954, 2012.

[4] S.-H. Fang, Y.-T. Hsu, and W.-H. Kuo, "Dynamic fingerprinting combination for improved mobile localization," *IEEE Transactions on Wireless Communications*, vol. 10, no. 12, pp. 4018–4022, 2011.

[5] Y. Yuan, J. Zhao, C. Qiu, and W. Xi, "Estimating Crowd Density In An RF-Based Dynamic Environment," *IEEE Sens. J.*, vol. 13, pp. 3837–3845, Oct 2013.

[6] S.-H. Fang, J.-C. Chen, H.-R. Huang, and T.-N. Lin, "Metropolitan-scale location estimation using FM radio with analysis of measurements," in *IEEE International Wireless Communications and Mobile Computing Conference*, pp. 171–176, 2008.

[7] P. Bahl and V. N. Padmanabhan, "RADAR: An In-Building RF-Based User Location and Tracking System," in *INFOCOM*, vol. 2, pp. 775–784, March 2000.

[8] S. Mahfouz, F. Mourad-Chehade, P. Honeine, J. Farah, and H. Snoussi, "Non-Parametric and Semi-Parametric RSSI/Distance Modeling for Target Tracking in Wireless Sensor Networks," *IEEE Sens. J.*, vol. 16, April 2016.

[9] H. Liu, H. Darabi, P. Banerjee, and J. Liu, "Survey of Wireless Indoor Positioning Techniques and Systems," *IEEE Trans Syst. Man Cybern C*, vol. 37, pp. 1067–1080, Nov 2007.

[10] I. T. Haque and C. Assi, "Profiling-Based Indoor Localization Schemes," *IEEE Syst. J.*, vol. 9, pp. 76–85, March 2015.

[11] T.-N. Lin, S.-H. Fang, W.-H. Tseng, C.-W. Lee, and J.-W. Hsieh, "A group-discrimination-based access point selection for WLAN fingerprinting localization," *IEEE Transactions on Vehicular Technology*, vol. 63, no. 8, pp. 3967–3976, 2014.

[12] S.-H. Fang, B.-C. Lu, and Y.-T. Hsu, "Learning location from sequential signal strength based on GSM experimental data," *IEEE Transactions on Vehicular Technology*, vol. 61, no. 2, pp. 726 –736, 2012.

[13] B. Mukhopadhyay, S. Sarangi, and S. Kar, "Performance Evaluation of Localization Techniques in Wireless Sensor Networks Using RSSI and LQI," in *NCC*, pp. 1–6, Feb 2015.

[14] S. Y. Cho, "Measurement Error Observer-Based IMM Filtering for Mobile Node Localization Using WLAN RSSI Measurement," *IEEE Sens. J.*, vol. 16, April 2016.

[15] C. Yang and H. R. Shao, "WiFi-Based Indoor Positioning," *IEEE Communications Magazine*, vol. 53, pp. 150–157, March 2015.

[16] A. S. Paul and E. A. Wan, "RSSI-Based Indoor Localization and Tracking Using Sigma-Point Kalman Smoothers," *IEEE J. Select. Topics Signal Process*, vol. 3, pp. 860–873, Oct 2009.

[17] L. H. Chen, E. H. K. Wu, M. H. Jin, and G. H. Chen, "Homogeneous Features Utilization To Address The Device Heterogeneity Problem In Fingerprint Localization," *IEEE Sens. J.*, vol. 14, pp. 998–1005, April 2014.

[18] S.-H. Fang, C.-C. Chuang, and C. Wang, "Attack-resistant wireless localization using an inclusive disjunction model," *IEEE Transactions on Communications*, vol. 60, no. 5, pp. 1209–1214, 2012.

[19] C. C. Huang and H. N. Manh, "RSS-Based Indoor Positioning Based on Multi-Dimensional Kernel Modeling and Weighted Average Tracking," *IEEE Sens. J.*, vol. 16, pp. 3231–3245, May 2016.

[20] S.-H. Fang and T.-N. Lin, "Robust wireless lan location fingerprinting by SVD-based noise reduction," in *IEEE International Symposium on Communications, Control and Signal Processing*, pp. 295–298, 2008.

[21] P. Xia, S. Zhou, and G. B. Giannakis, "Adaptive MIMO-OFDM Based On Partial Channel State Information," *IEEE Trans. Signal Process.*, vol. 52, pp. 202–213, Jan 2004.

[22] A. F. Molisch, *Orthogonal Frequency Division Multiplexing (OFDM)*, pp. 417–443. Wiley-IEEE Press, 2011.

[23] D. Halperin, W. Hu, A. Sheth, and D. Wetherall, "Tool Release: Gathering 802.11n Traces With Channel State Information," *SIGCOMM Comput. Commun. Rev.*, Jan 2011.

[24] S. Sen, R. R. Choudhury, B. Radunovic, and T. Minka, "Precise Indoor Localization Using PHY Layer Information," in *ACM HotNets*, pp. 18:1–18:6, 2011.

[25] F. Adib, H. Mao, Z. Kabelac, D. Katabi, and R. C. Miller, "Smart Homes that Monitor Breathing and Heart Rate," in *in Proceedings of the Annual ACM Conference on Human Factors in Computing Systems*, pp. 837–846, April 2015.

[26] C. Han, K. Wu, Y. Wang, and L. M. Ni, "WiFall: Device-Free Fall Detection by wireless Networks," in *IEEE Conference on Computer Communications*, pp. 271–279, April 2014.

[27] Z. Yang, Z. Zhou, and Y. Liu, "From RSSI To CSI: Indoor Localization Via Channel Response," *ACM Comput. Surv.*, vol. 46, no. 2, pp. 25:1–25:32, November 2013.

[28] K. Wu, J. Xiao, Y. Yi, D. Chen, X. Luo, and L. Ni, "CSI-Based Indoor Localization," *IEEE Trans. Parallel Distrib. Syst.*, vol. 24, no. 7, pp. 1300–1309, July 2013.

[29] Z.-P. Jiang, W. Xi, X. Li, S. Tang, J.-Z. Zhao, J.-S. Han, K. Zhao, Z. Wang, and B. Xiao, "Communicating Is Crowdsourcing: Wi-Fi Indoor Localization With CSI-Based Speed Estimation," *JCST*, vol. 29, no. 4, pp. 589–604, 2014.

[30] D. Chen, L. Du, Z. Jiang, W. Xi, J. Han, K. Zhao, J. Zhao, Z. Wang, and R. Li, "A Fine-Grained Indoor Localization Using Multidimensional Wi-Fi Fingerprinting," in *ICPADS*, pp. 494–501, Dec 2014.

[31] X. Wang, L. Gao, S. Mao, and S. Pandey, "DeepFi: Deep Learning for Indoor Fingerprinting Using Channel State Information," in *Proc. IEEE WCNC*, pp. 1666–1671, March 2015.

[32] X. Wang, L. Gao, S. Mao, and S. Pandey, "CSI-Based Fingerprinting for Indoor Localization: A Deep Learning Approach," *IEEE Trans Veh Technol*, vol. PP, no. 99, pp. 1–1, 2016.

[33] F. Wen and C. Liang, "Fine-Grained Indoor Localization Using Single Access Point With Multiple Antennas," *IEEE Sens. J.*, vol. 15, pp. 1538–1544, March 2015.

[34] J. Xiao, K. Wu, Y. Yi, and L. Ni, "FIFS: Fine-Grained Indoor Fingerprinting System," in *ICCCN*, pp. 1–7, July 2012.

[35] K. Wu, J. Xiao, Y. Yi, M. Gao, and L. Ni, "FILA: Fine-Grained Indoor Localization," in *INFOCOM*, pp. 2210–2218, March 2012.

[36] Y. Chapre, A. Ignjatovic, A. Seneviratne, and S. Jha, "CSI-MIMO: Indoor Wi-Fi Fingerprinting System," in *Proc. IEEE LCN*, pp. 202–209, Sept 2014.

[37] Y. Chapre, A. Ignjatovic, A. Seneviratne, and S. Jha, "CSI-MIMO: An Efficient Wi-Fi Fingerprinting Using Channel State Information With MIMO," *Pervasive and Mobile Computing*, vol. 23, pp. 89–103, July 2015.

[38] M. Kotaru, K. Joshi, D. Bharadia, and S. Katti, "SpotFi: Decimeter Level Localization Using WiFi," in *SIGCOMM*, pp. 269–282, 2015.

[39] C. Wu, Z. Yang, Z. Zhou, X. Liu, Y. Liu, and J. Cao, "Non-Invasive Detection of Moving and Stationary Human with WiFi," *IEEE Journal on Selected Areas in Communications*, vol. 33, pp. 2329–2342, Nov 2015.

[40] S. Mallat, "A Theory for Multiresolution Signal Decomposition: The Wavelet Representation," *IEEE Trans. Knowl. Data Eng.*, pp. 674–693, 1989.

[41] S. G. Mallat, "Multifrequency Channel Decompositions of Images and Wavelet Models," *IEEE Transactions on Acoustis, Speech and Signal Processing*, vol. 37, pp. 2091–2110, Dec 1989.

[42] M. Vetterli and J. Kovacevic, *Wavelets and Subband Coding*. Prentice-Hall, Inc., 1995.

[43] S. S. Wang, J. W. Hung, and Y. Tsao, "A Study On Cepstral Sub-Band Normalization for Robust ASR," in *Proc. ISCSLP*, pp. 141–145, Dec 2012.

[44] P.-Y. Chen, "VLSI Implementation for One-Dimensional Multilevel Lifting-Based Wavelet Transform," *IEEE Trans. Comput.*, vol. 53, no. 4, pp. 386–398, 2004.

[45] A. de la Torre, A. M. Peinado, J. C. Segura, J. L. Perez-Cordoba, M. C. Benitez, and A. J. Rubio, "Histogram Equalization of Speech Representation for Robust Speech Recognition," *IEEE Trans. Speech Audio Processing*, vol. 13, pp. 355–366, May 2005.

[46] S. H. Fang, C. H. Wang, and Y. Tsao, "Compensating for Orientation Mismatch In Robust Wi-Fi Localization Using Histogram Equalization," *IEEE Trans. Veh. Technol.*, vol. 64, pp. 5210–5220, Nov 2015.

[47] M. A. Youssef, A. Agrawala, and A. Udaya Shankar, "WLAN Location Determination via Clustering and Probability Distributions," in *Proc. IEEE PerCom*, pp. 143–150, 2003.

[48] A. Cohen, I. Daubechies, and J.-C. Feauveau, "Biorthogonal Bases of Compactly Supported Wavelets," *Commun. Pure Appl. Math.*, vol. 45, no. 5, pp. 485–560, 1992.

[49] M. Antonini, M. Barlaud, P. Mathieu, and I. Daubechies, "Image Coding Using Wavelet Transform," *IEEE Trans. Image Processing*, vol. 1, pp. 205–220, Apr 1992.

[50] G. Strang and T. Nguyen, *Wavelets and Filter Banks*. Wellesley-Cambridge Press, 1996.

[51] F. Hilger and H. Ney, "Quantile Based Histogram Equalization for Noise Robust Large Vocabulary Speech Recognition," *IEEE Trans. Audio, Speech, and Language Processing*, vol. 14, pp. 845–854, May 2006.

Shih-Hau Fang (M'07-SM'13) received a B.S. from National Chiao Tung University in 1999, an M.S. and a Ph.D. from National Taiwan University, Taiwan, in 2001 and 2009, respectively, all in communication engineering. From 2001 to 2007, he was a software architect at Internet Services Division at Chung-Hwa Telecom Company Ltd.. In 2009, he joined the Department of Electrical Engineering, Yuan Ze University, where he is currently an Associate Professor. He is also technical advisor to HyXen Technology Company Ltd. and serves as an Associate Editor for IEICE Trans. on Information and Systems. Prof. Fang received the YZU Young Scholar Research Award in 2012 and the Project for Excellent Junior Research Investigators, Ministry of Science and Technology in 2013. His research interests include indoor positioning, mobile computing, machine learning, and signal processing. He is a senior member of IEEE.

Wei-Hsiang Chang received the B.S. degree in manufacturing engineering and management technologies and the M.S. degree in electrical engineering from Yuan Ze University, Taoyuan, Taiwan, in 2008 and 2016, respectively. From 2005 to 2006, he was mechanism design engineer at Chun Chin Automatic Ltd. From 2007 to 2012, he was an engineer at HTC Corporation responsible for system quality test and verification. His research interests include pattern recognition, multivariable analysis and indoor localization.

Yu Tsao received the B.S. and M.S. degrees in electrical engineering from National Taiwan University, Taipei, Taiwan, in 1999 and 2001, respectively, and the Ph.D. degree in electrical and computer engineering from Georgia Institute of Technology, Atlanta, GA, USA, in 2008. From 2009 to 2011, he was a Researcher with the National Institute of Information and Communications Technology, Kyoto, Japan, where he was engaged in research and product development in automatic speech recognition for multilingual speech-to-speech translation. He is currently an Associate Research Fellow with the Research Center for Information Technology Innovation, Academia Sinica, Taiwan. His research interests include speech recognition, audio-coding, deep neural networks, bio-signals, and acoustic modeling.

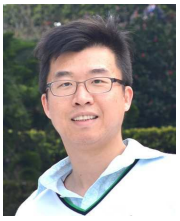

Huang-Chia Shih (M08) received the B.S. degree (Hons.) in electronics engineering from the National Taipei University of Technology, Taipei, Taiwan, in 2000, and the M.S. and Ph.D. degrees in electrical engineering (EE) from the National Tsing Hua University in 2002 and 2008, respectively. He served as a visiting scholar with the department of EE, University of Washington from 2006 to 2007. He was a visiting professor with the John von Neumann Faculty of Informatics, Obuda University, Hungary in 2011. He has been an associate professor with the department of EE, Yuan Ze University (YZU), Taoyuan, Taiwan, since 2016. He has authored over 50 technical papers in refereed journals and conference proceedings. His research interests are content-based multimedia processing, pattern recognition, and humancomputer interaction. He received the Outstanding Youth Electrical Engineer Award from the Chinese Institute of Electrical Engineering in 2015, the YZU Young Scholar Research Award from YZU in 2015, the Kwoh-Ting Li Young Researcher Award from ACM Taipei/Taiwan Chapter in 2014, the Pan Wen Yuan Exploration Research Award from Pan Wen Foundation in May 2013, the best paper awards from IEEE-ISCE 2013, and the IEEE-GCCE 2015.

Chiapin Wang (M08-SM14) received the B.S. degree in electrical engineering from National Cheng Kung University in 1994, and M.S. and Ph.D. degrees from National Taiwan University in 2003 and 2008, respectively, both in the graduate institute of communication engineering. After his military services in 1996, he worked as a hardware/firmware engineer in Tatung Telecom. Co., Ltd., Taipei for three years, and was responsible for the design of IC card public payphone. From 1999 to 2006, he worked as a researcher in the Telecommunication Laboratories at Chunghwa Telecom Co., Ltd., Taoyuan, Taiwan, where he investigated related techniques on IC card appliances. From 2006 to 2007, he worked as a field engineer in the Enterprise Business Group, Chunghwa Telecom Co., Ltd., and was responsible for the construction of digital home system. Since August 2008, he has been with the department of electrical engineering, National Taiwan Normal University. His research interests include network performance analysis and wireless networks. Dr. Wang is a senior member of IEEE.